**Original Research**

# High-Resolution Diffusion-Weighted Imaging With Interleaved Variable-Density Spiral Acquisitions

Tie-Qiang Li, PhD,[1]* Dong-Hyun Kim, PhD,[2] and Michael E. Moseley, PhD[2]

**Purpose:** To develop a multishot magnetic resonance imaging (MRI) pulse sequence and reconstruction algorithm for diffusion-weighted imaging (DWI) in the brain with submillimeter in-plane resolution.

**Materials and Methods:** A self-navigated multishot acquisition technique based on variable-density spiral k-space trajectory design was implemented on clinical MRI scanners. The image reconstruction algorithm takes advantage of the oversampling of the center k-space and uses the densely sampled central portion of the k-space data for both imaging reconstruction and motion correction. The developed DWI technique was tested in an agar gel phantom and three healthy volunteers.

**Results:** Motions result in phase and k-space shifts in the DWI data acquired using multishot spiral acquisitions. With the two-dimensional self-navigator correction, diffusion-weighted images with a resolution of $0.9 \times 0.9 \times 3$ mm$^3$ were successfully obtained using different interleaves ranging from 8–32. The measured apparent diffusion coefficient (ADC) in the homogenous gel phantom was $(1.66 \pm 0.09) \times 10^{-3}$ mm$^2$/second, which was the same as measured with single-shot methods. The intersubject average ADC from the brain parenchyma of normal adults was $(0.91 \pm 0.01) \times 10^{-3}$ mm$^2$/second, which was in a good agreement with the reported literature values.

**Conclusion:** The self-navigated multishot variable-density spiral acquisition provides a time-efficient approach to acquire high-resolution diffusion-weighted images on a clinical scanner. The reconstruction algorithm based on motion correction in the k-space data is robust, and measured ADC values are accurate and reproducible.

**Key Words:** diffusion-weighted imaging; self-navigator; motion correction; interleaved variable-density spiral acquisition; high-resolution MRI
**J. Magn. Reson. Imaging 2005;21:468–475.**
**Published 2005 Wiley-Liss, Inc.**†

THE CLINICAL UTILITY OF DIFFUSION-weighted imaging (DWI) for rapid assessment of acute stroke (1) has been well established. The extension of DWI into diffusion tensor imaging (DTI) to explore the diffusion anisotropy has recently become a promising technique for noninvasive mapping of neuronal connectivity in the living human brain (2–5). This technique is also very useful for detecting abnormalities in white matter integrity, composition, and development caused by neurological and psychiatric disorders (5,6). However, the potential of this technique to study complex and detailed cerebral connectivity is greatly limited by the low spatial resolution and poor signal-to-noise ratio (SNR) of the most commonly used single-shot imaging techniques. Improving the spatial resolution and SNR of DWI is of great importance for the detailed mapping of the complex neuronal pathways in the brain with DTI. The lack of spatial resolution and SNR also pose severe limitations for its clinical applications, because it is difficult to detect minor structural changes in the white matter associated with brain disorders.

The limited spatial resolution of diffusion-weighted images is inherently associated with the severe motion sensitivity of DWI. The large displacement encoding gradient pulses applied in DWI measurements are not only sensitive to the microscopic random molecular motions, but also very sensitive to the physiological motions in the brain, such as cardiac- and respiratory-driven pulsations, cerebral spinal fluid (CSF) flow, and involuntary body movements. Neither can the effect of vibration induced by the strong diffusion-weighting gradients be ignored, as evidenced by the severe artifacts observed in DWI of gel phantoms. DWI pulse sequences descendent from single-shot magnetic resonance imaging (MRI) techniques, such as echo-planar imaging (EPI) (1,6,7), spiral imaging (8–10), and fast spin echo (FSE) (11,12), are less prone to motion arti-

[1]Laboratory of Functional and Molecular Imaging, National Institute of Neurological Disease and Stroke, National Institute of Health, Bethesda, Maryland, USA.

[2]Radiology Sciences Laboratory, Department of Radiology, Stanford University, Stanford, California, USA.

Contract grant sponsor: Whitaker Foundation; Contract grant number: RG-02-0085; Contract grant sponsor: National Institutes of Health; Contract grant number: MH063455-01A1R01.

This paper has been orally presented at ISMRM 2003, Toronto (abstract 69).

*Address reprint requests to: T.-Q.L., Laboratory of Functional and Molecular Imaging, NINDS/NIH, 10 Center Dr., Room 10/B1D720, Bethesda, MD 20892. E-mail: litie@ninds.nih.gov

Received May 4, 2004; Accepted December 17, 2004.
DOI 10.1002/jmri.20287
Published online in Wiley InterScience (www.interscience.wiley.com).

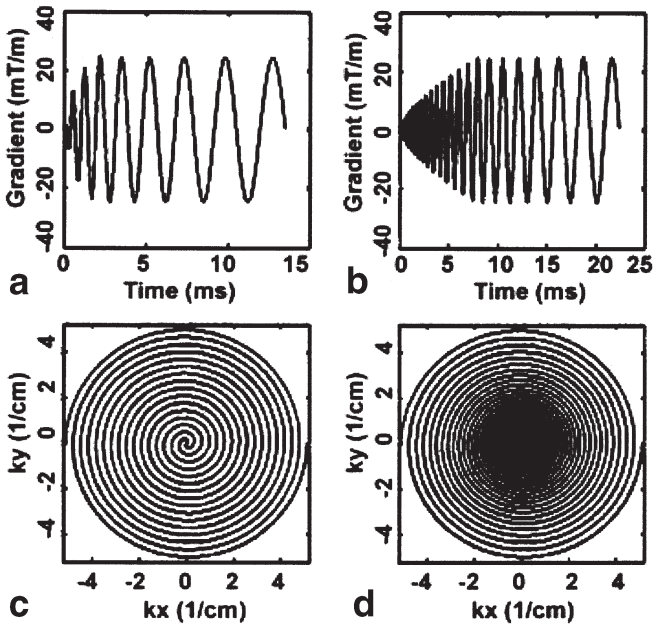


**Figure 1.** The readout gradient waveform (**a** and **b**) of the first interleave as well as the k-space trajectories (**c** and **d**) for the first and ninth interleaves for acquiring images with FOV = 230 mm and 256 × 256 in-plane resolution using 16 interleaved spiral acquisitions. The designs for uniform (a and c) and variable-density trajectory (b and d) are shown for a gradient system with a gradient amplitude of 40 mT/m and a slew rate of 200 T/m/second.

facts when the entire readout is carried out in a short period (~100 msec). The typical spatial resolution for DWI derived from the single-shot techniques is about $2 \times 2 \times 4$ mm$^3$. The SNR for a diffusion-weighted image acquired using a 1.5-T clinical scanner with a b-value of 1000 seconds/mm$^2$ is close to 10. With the single-shot technique, susceptibility artifacts can also be problematic in the basal region of the brain. To achieve higher in-plane spatial resolution, multishot techniques, in combination with the acquisition of navigation signals to correct for motion artifacts, have to be employed (7,12–15). Since pulse sequences based on conventional k-space sampling provide limited time efficiency (13,14), multishot techniques based on EPI (7) and FSE (12) have recently been proposed. For example, Butts et al (7) combined a two-dimensional spiral navigator with interleaved EPI to acquire high-resolution diffusion-weighted images in stroke patients. Pipe et al (12) used a PROPELLER sequence based on self-navigated multishot FSE for high-resolution DWI in the brain.

In this study, a time-efficient approach based on self-navigated variable-density spiral to acquire robust high-resolution diffusion-weighted images was investigated. Spiral trajectory has been very attractive for high-resolution MRI of moving objects because of its overall merits against motion artifacts and the capability to use the readout itself as a navigator (9,16–18). However, with the constant-density spiral trajectory design (Fig. 1), the estimate of phase errors between interleaves using a single central k-space data point is not very reliable. The inadequate phase compensation between interleaves can result in nonuniform sampling of k-space and render the diffusion-weighted images with severe motion artifacts (19). In the present study, we implemented a variable-density spiral trajectory design to adequately oversample the inner k-space portion (the first 100 data points of each interleave covering less than 0.5% of the k-space radius). With this design, the motion-induced phase shift and k-space offset between interleaves can be reliably estimated from multiple data points in a least-squares sense. Another advantage of this method is that the trajectory can be calculated using a simplified analytical solution (8,20), which enables flexible prescription of the scanning parameters.

## MATERIALS AND METHODS

The proposed imaging method includes three steps: 1) variable-density spiral data acquisition, 2) self-navigated motion correction, and 3) imaging reconstruction. The details for each step are discussed below.

### *Design of the Variable-Density Spiral Trajectory*

The design of the variable-density trajectory is usually accomplished by feeding the desired sampling density profile into a gradient waveform design algorithm. In the present study, the spiral trajectory was designed using the following empirical approximation:

$$k(\tau) = (N/2/FOV)\tau^{\alpha} \exp(i2\pi n\tau) \qquad (1)$$

where N and FOV are the matrix size and field of view of the image, respectively. $\alpha$ is an empirical parameter that determines the degree of oversampling near the origin and is typically in the range of $\alpha \approx (2,6)$. $n$ is the number of turns in the k-space trajectory.

A typical spiral trajectory will start off in the slew-rate-limited region. After reaching its maximum gradient amplitude, it will switch to the amplitude-limited region. Following the piecewise approximation approach proposed by Glover (8,20), the above variable-density spiral trajectory can be analytically calculated using the following equations:

$$\tau(t) = \begin{cases} \left[ \sqrt{\frac{S_m\gamma}{\lambda\omega^2}} (\alpha/2 + 1)t \right]^{1/(1+\alpha/2)} & 0 \le t \le t_c \\ \left[ \frac{\gamma g_m}{\lambda\omega} (1+\alpha)t \right]^{1/(1+\alpha)} & t_c \le t \le t_{end} \end{cases} \qquad (2)$$

where $g_m$ and $s_m$ are the maximum gradient amplitude and maximum gradient slew rate, respectively. $\lambda$ = N/FOV, $\omega = 2\pi n$, $\gamma$ is the proton gyromagnetic ratio, and $t_c$ represents the time point when the trajectory changes from a slew-rate-limited regime to an amplitude-limited regime. A detailed analysis of the design has been given elsewhere (20). It is worthwhile to point out that the $\alpha$ parameter determines the extent of oversampling near the k-space origin. For example, when $\alpha = 1$, this will be a constant-density trajectory as described in Glover (8). Larger values of $\alpha$ will result in a higher degree of oversampling at the cost of off-reso-

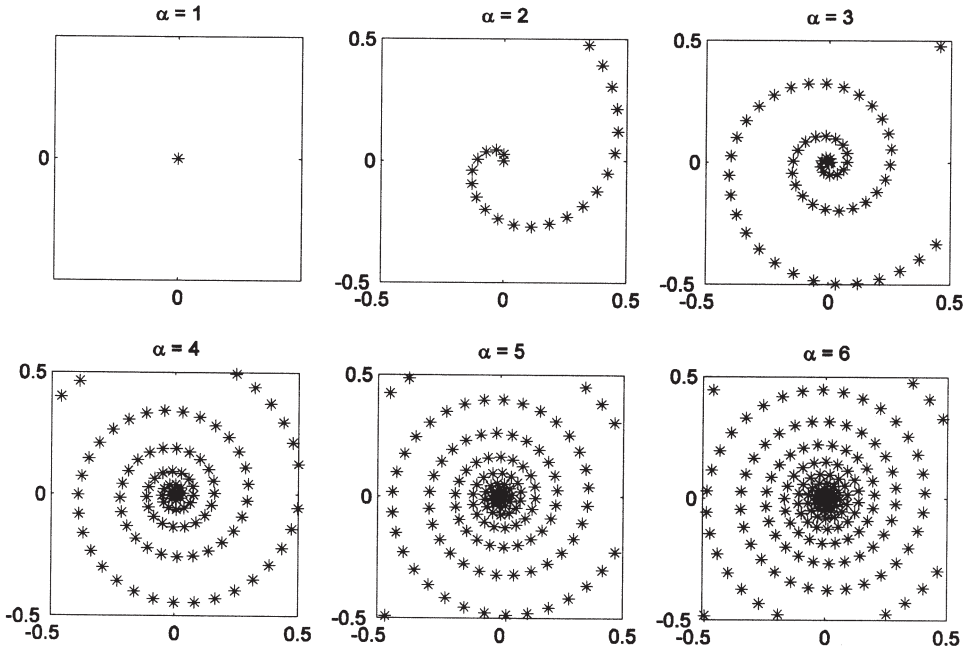


**Figure 2.** k-space sampling points for various values of α. The inner 0.5% of the maximum k-space value is plotted. For DWI, the oversampling of inner k-space is crucial due to the associated sensitivity to motions. Although larger values of α can provide higher degrees of oversampling, the trajectory will suffer from off-resonance effects due to longer readouts. In this work, we have empirically selected α = 4.

nance effects due to a longer readout. Figure 2 illustrates this by plotting the sampling point within the center 0.5% of the k-space trajectory for a 256 × 256 acquisition over an FOV = 230 mm using 16 interleaves. In this study, α = 4 was used to achieve adequate oversampling for robust motion corrections.

The acquisitions of different interleaves were implemented by taking advantage of the rotation matrix subroutine for the gradient waveforms. Once the readout gradient waveforms for the unrotated first interleave were computed as described above, the readout gradient waveforms for the other interleaves were obtained at the run time from the unrotated gradient waveforms by multiplying with the corresponding rotation matrices. The rotation angle for the i-th interleave for a design with a total of m interleaves is equal to $\frac{2\pi}{m}(i - 1)$, where $1 \leq i \leq m$

### *Self-Navigated Motion Correction*

Motions during the application of diffusion-weighting gradients result in three-dimensional k-space displacements, which are difficult to be theoretically predicted. Both the phase shifts and k-space offsets need to be measured and compensated for individual interleaves before combining the data to construct a high-resolution diffusion-weighted image. It is necessary to implement at least a two-dimensional navigator motion correction mechanism for acquiring diffusion-weighted images with multishot acquisitions. This is accomplished by using the oversampled initial portion of each spiral readout as a self-navigator.

To estimate the motion-induced phase shift and k-space displacement of the data, a least-squares fitting algorithm was implemented by fitting a two-dimensional sinc function to the adequately oversampled portion of the k-space modulus data. The k-space coordinate offsets from the origin and phase of the peak signal were assigned as the k-space displacement and phase shift of the signal, respectively. We also tested the method used by Butts et al (7), in which a signal intensity-weighted average phase value was estimated based on the points located within the main lobe of the k-space data. The results from the later method were somewhat dependent on the weighting method and the intensity threshold used to select the data points.

The correction of the k-space displacement was performed by using the actual in-plane k-space trajectory in the gridding procedure. In the absence of motion, the designed center k-space path should coincide from view to view in multishot spiral acquisitions. With motions, the actual k-space trajectory should be the designed trajectory plus the estimated deviations. Gridding with the actual k-space path can therefore compensate the effects of motions. Out-of-plane motions can result in k-space offsets in the third dimension. To mitigate the out-of-plane motion artifacts using a two-dimensional in-plane navigator mechanism, a provisionary measure was implemented, which excludes an entire interleave when the signal is so corrupted that its intensity is less than 70% of the maximum of all interleaves.

### *Image Reconstruction*

When the k-space data do not fall on the Cartesian linear grid, as is the case with spiral trajectory in addition to the arbitrary motion-induced deviations, gridding interpolation is one of the most widely used image reconstruction methods. The gridding interpolation was performed off-line on a Sun workstation using the method described by Meyer et al (16). To compensate for the nonuniform k-space sampling density of the data acquisition, a nonlinear weighting was applied to the raw data. The compensation function used here was based on the absolute value of the Jacobian determinant in the transformation to Cartesian coordinates from the spiral trajectory, along which data were actu-

ally acquired (10). The actual k-space path was calculated as the sum of designed trajectory and the estimated deviation from the self-navigator. The convolution kernel for gridding was a two-dimensional Kaiser-Bessel function with a fixed width of 1.5/FOV to convolve the raw data sampled in spiral trajectories onto a two-dimensional doubly oversampled square matrix.

After applying a window function that matches the designed variable-density spiral profile, a two-dimensional fast Fourier transformation (FFT) was performed to produce the image in real space. When the applied window function is proportional to the sampling density, the general theory of variable-density sampling illustrates that the side lobes in the point-spread function can be reduced without an increase in the noise variance (21). It should be noted that the sampling radius has to be doubled to preserve the same SNR and resolution when the window function is applied. This is also the case for uniform spiral design. Before the computation of the amplitude image, the complex image was rescaled by the Fourier transformation of the gridding kernel to correct the image intensity modulation caused by the convolution. Our reconstruction routine also used a $B_0$ field map acquired at the beginning of the diffusion experiment to correct for linear shim terms and carrier frequency offsets in each slice.

### *Experimental*

The diffusion-weighted MRI pulse sequence with variable-density spiral trajectory was implemented on GE Signa 1.5-T and 3-T whole-body MRI scanners using the EPIC LX 9.0 platform. Since both scanners were equipped with the same gradient hardware, which can provide the maximum gradient strength of 40 mT/m and the slew rate of 200 T/m/second, the implementation was transparent on both systems and the scanning protocols were also the same. For comparison, with a given acquisition prescription, the sequence has the option to choose either a variable- or constant-density spiral trajectory. The sequence was first tested using an agar gel phantom at b = 600 seconds/mm$^2$ and a matrix size of 256 × 256. The tests included image quality and diffusion coefficient reproducibility using different number of spiral interleaves. In vivo measurements were then performed in three male volunteers (aged between 32 and 38 years old) using the following protocol: b = 1000 seconds/mm$^2$, matrix size = 256 × 256, FOV = 230 mm, slice thickness = 3 mm, NEX = 1, TE/TR = 80/6000 msec, acquisition bandwidth = 100 kHz, and four different diffusion-weighting directions (xyz, –x–y+z, x–y–z, –x+y–z). For quantification of the apparent diffusion coefficient (ADC), the average result from the four diffusion-weighting gradient directions was used. It has been shown (22) that the average is proportional to the trace value of the diffusion tensor and independent of the direction of the diffusion-weighting gradient. The maximum available gradient strength was used for each diffusion-weighting gradient with $\delta$ = 35.1 msec and $\Delta$ = 35.5 msec. Three different designs based on 8, 16, and 32 interleaves were used for the spiral readout gradient waveforms. The durations of the readout gradient for uniform and variable-density acquisitions are listed in Table 1. Although the radius of k-space coverage for the uniform and variable-density spiral was about the same, the readout duration for the variable-density spiral was 50% to 70% longer due to the oversampling in the center. Each subject completed six sets of DWI measurements using three different interleaves combined with uniform and variable-density spiral waveforms on both 1.5-T and 3-T scanners. Three repeated measurements were performed for each set of data acquisition parameters. The experiment on each scanner lasted for about 2 1/2 hours for each subject.

Table 1
The Length of Spiral Readout fo 8, 16, and 32 Interleave (*N*)

| Interleaves (*N*) | Interleave (uniform)[a] | Duration (msec) (variable)[b] |
|---|---|---|
| 8 | 26.74 | 46.30 |
| 16 | 13.52 | 22.40 |
| 32 | 6.98 | 10.45 |

[a]For the case of $\alpha$ = 1.
[b]For the case of $\alpha$ = 4.

## RESULTS

As shown in Fig. 3, motions in DWI measurements can give rise to signal distortions in different fashions ranging from signal loss to k-space offset. With the two-dimensional self-navigator, the in-plane k-space offset can be reliably measured and corrected. As shown in Fig. 4, the k-space offsets for the majority of interleaves are in the range of $\Delta k = \pm 3/FOV$. The radius and density of the oversampled self-navigator at $\alpha$ = 4 are apparently adequate for reliable estimate of the k-space offsets associated with low to moderate degrees of motions during the application of diffusion-weighting gradients.

With the constant-density spiral trajectory, the diffusion-weighted MR images collected from the human brains (Fig. 5a and c) have severe motion artifacts. For this design, the motion correction navigator based on the phase error estimates from the first two data points in each interleave can reduce the motion artifacts somewhat. This is apparently not robust, as illustrated by comparing images in Fig. 5a with those in Fig. 5c. The interleaved spiral acquisitions with constant density cannot reliably measure ADC in the phantom and human brains. The variations between individual measurements were larger than 30%. With the variable-density trajectory design, the image quality of the diffusion-weighted image was improved even without implementing any motion correction scheme (Fig. 5b). As shown in Figs. 5d and 6, using a more robust motion correction method can progressively improve the image quality and SNR to a higher level. The average ADC ± SD for each data set collected using variable-density gradient waveforms at 3 T is summarized in Table 2. The SD for the in vivo measurements for individual

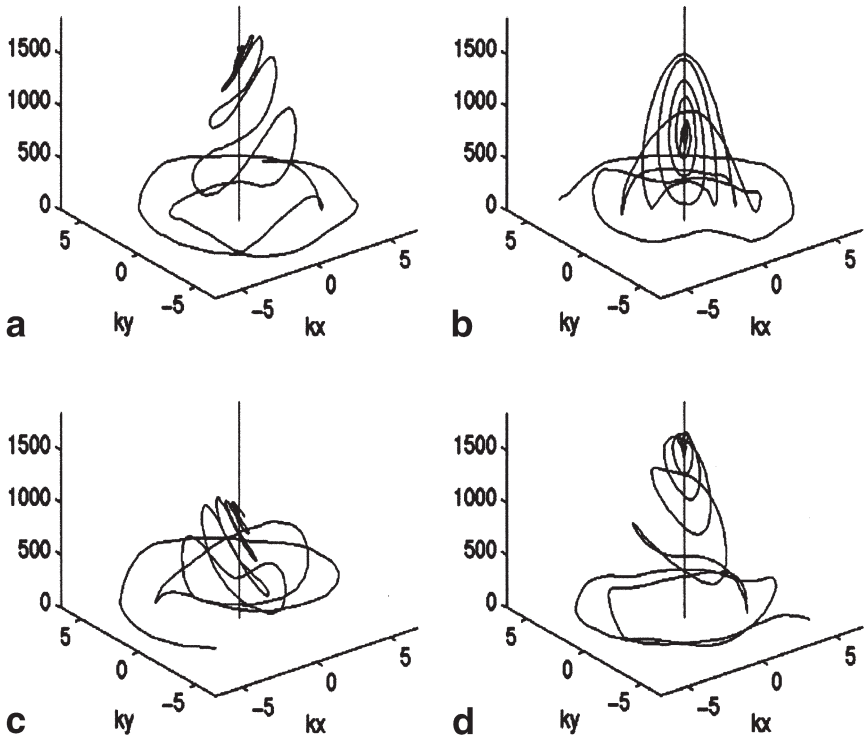


**Figure 3.** The center portion of k-space data as a function of k-space locations (1/FOV). The typical effects of motion on the time domain signal amplitude are illustrated as follows: slightly reduced signal amplitude with a relatively small k-space offset (**a**), relatively large signal reduction with a large k-space displacement (**b**), significant corruption of the signal (**c**), and negligible signal reduction and k-space offset (**d**). The data were acquired in a DWI experiment with b = 1000 seconds/mm$^2$ from the brain of a normal volunteer using the variable-density spiral trajectory ($\alpha$ = 4), 16 interleaves/image, FOV = 230 mm, and matrix size = 256 × 256.

subjects was about 8%, which is somewhat higher than the 5% for the phantom data. The average ADC measured in the homogenous gel phantom was (1.66 ± 0.09) × $10^{-3}$ mm$^2$/second, which was identical to what was measured with single-shot methods.

The images shown in Fig. 5d were acquired at 1.5 T using 16 interleaves. Figure 6 shows a typical set of images acquired at 3 T using 32 interleaves. As shown, shortening the readout duration in each interleave by increasing the number of interleaves reduces the local off-resonance effect (blurring). The average interindividual ADC in the normal brain tissue estimated from such measurement was (0.91 ± 0.01) × $10^{-3}$ mm$^2$/second, which is consistent with the literature values (1,7,10,12).

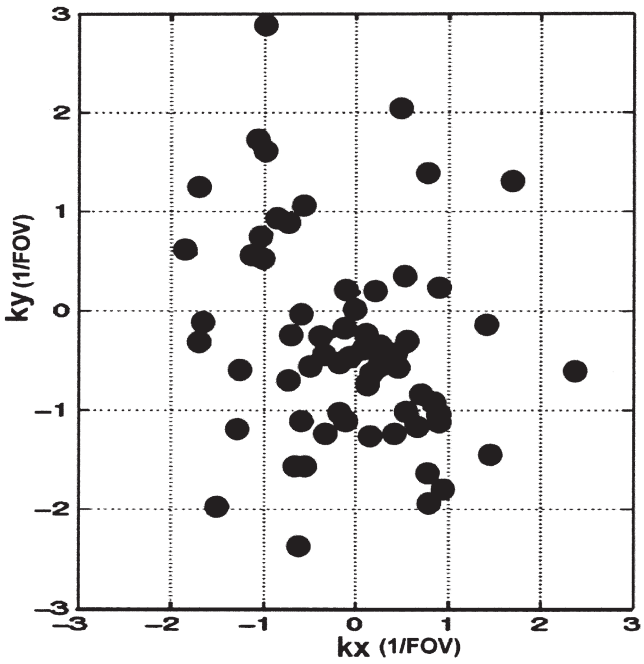


**Figure 4.** The displacements of the center k-space data point in 1/FOV for different interleaves due to motions during the application of diffusion-weighting gradients as estimated by searching for the data point corresponding to the maximum intensity in each interleave. Results for four successive time frames of DWI data acquired in a normal subject at b = 1000 seconds/mm$^2$ are shown.

## DISCUSSION

The variable-density spiral acquisition sequence is well suited for DWI because the inherent robustness of central out acquisition methods to motion artifacts (9). This is also attributable in part to oversampling of central k-space, which reduces artifacts in a similar manner as signal averaging with multiple acquisitions. Furthermore, starting data sampling from the origin of k-space greatly reduces the moment of imaging gradient in the central k-space and motion-induced image phase error (type II artifacts) (9,23). The advantages for implementing a simplified variable-density spiral trajectory design using a closed-form approximation for DWI are the following: 1) robust motion correction mechanism based on self-navigator signal, 2) high efficiency of data acquisition for high-resolution DWI, and 3) flexible applicability for different protocols and hardware. The main limitation, however, is that it cannot reliably correct the effect of through-plane motions, as in all other two-dimensional acquisition methods. The out-of-plane motion can cause significant signal reduction, and this

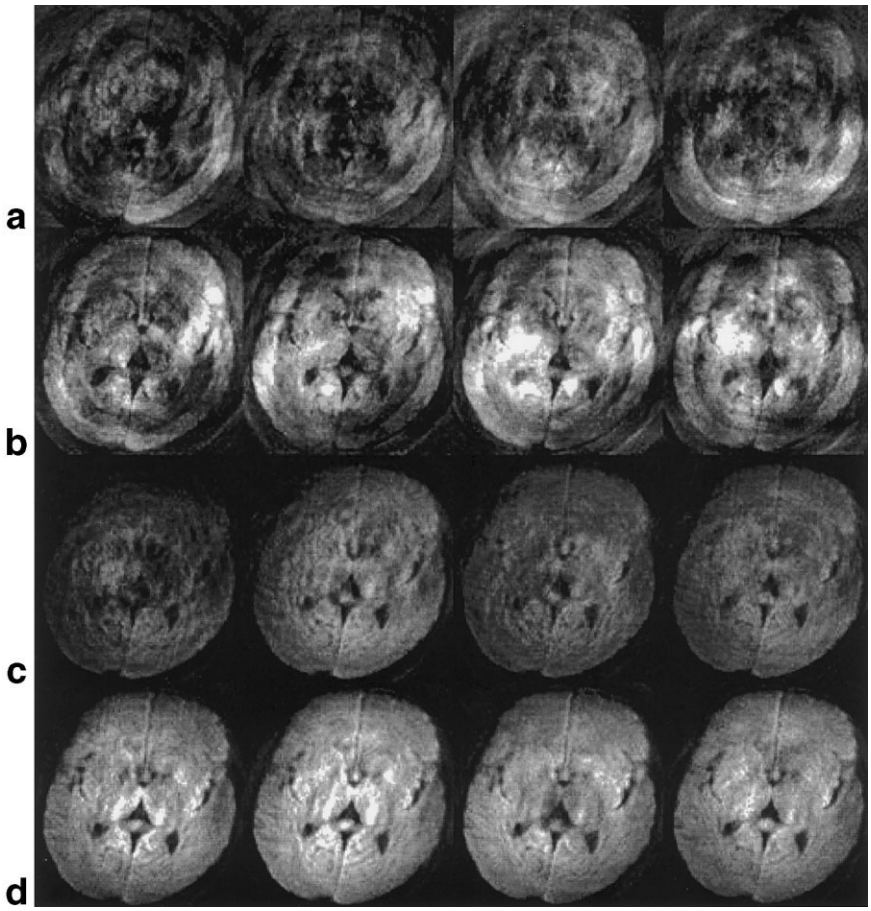


**Figure 5.** Comparison of diffusion-weighted images (FOV = 230 mm, matrix size = 256 × 256) acquired in the transverse plane using 16 interleaved spiral readouts with the constant- (**a** and **c**) and variable- (**b** and **d**) density trajectory designs. Without implementation of self-navigated motion correction, motion artifacts render the images useless (a and b). The motion artifacts in the images (c and d) are reduced by applying even a simple motion correction mechanism based on the first two data points in each interleave. The four different images in each row were acquired using four different diffusion-weighting gradient directions (the tetrahedral set: xyz, –x–y+z, x–y–z, –x+y–z), respectively.

can be particularly problematic in brain regions where cardiac and respiratory pulsations are most active. The data rejection based on signal peak intensity removes the worst affected interleaves, but it does not correct the remaining interleaves on the phase errors associated with out-of-plane motions.

It was recently suggested that motion correction in the imaging space might be needed to correct for nonlinear phase effect (12,19,24). One necessary condition to perform image space phase correction is that a complete image must be constructed from each interleave of the multishot acquisition. Depending on the acquisition strategy, the image constructed from a subset of the complete data set can exhibit either blurring or aliasing. For example, if each subset is densely sampled ($\Delta k = 1/FOV$), with a rotating band passing the center of k-space as in the PROPELLER sequence (12), the constructed image will be simply blurred with limited resolution and the phase correction in the image space can be adequately done after removing the ringing. If each subset covers the entire k-space but does not sample as sufficiently dense as the variable-density spiral scans used here, the signal will be averaged globally and the constructed image from a single interleave generally contains aliased high-frequency artifacts. In this case, the image-based correction cannot be done correctly and the correction algorithm based on k-space data is more adequate. It is possible to construct an image of very low resolution from each spiral interleave based on the oversampled portion of the data. However, this would require a significant portion of each interleave to be densely sampled.

Given the limited imaging time available in clinical situations such as acute stroke, time efficiency is a very relevant issue for DWI sequence development. The interleaved variable-density spiral method is extremely time efficient; whole-brain diffusion-weighted image data set up to 50 slices can be acquired within three minutes using a TR of five seconds and 32 interleaves. Time efficiency is also essential for DTI and Q-space imaging, which require multiple diffusion-weighting directions and b-values. In most clinical stroke studies (1,10), ADC measurements were typically conducted using two points of different b-values. When image degradation due to increased sensitivity to motion artifacts and susceptibility artifacts is not considered (25), the optimum SNR in ADC is obtained by choosing $b = 1.1/ADC$. For normal brain tissues, this requires a b-value of about 1000 seconds/mm$^2$, as used for the in vivo measurements in this work. The formation of average ADC maps from multiple measurements using an appropriate distributed gradient set (26) may help improve SNR and remove the effects of white matter anisotropy desirable for clinical diagnostics.

Improving the spatial resolution, reducing imaging artifacts, and optimizing SNR for DWI are important issues both for clinical application and for detailed mapping of the complex neuronal pathways in the

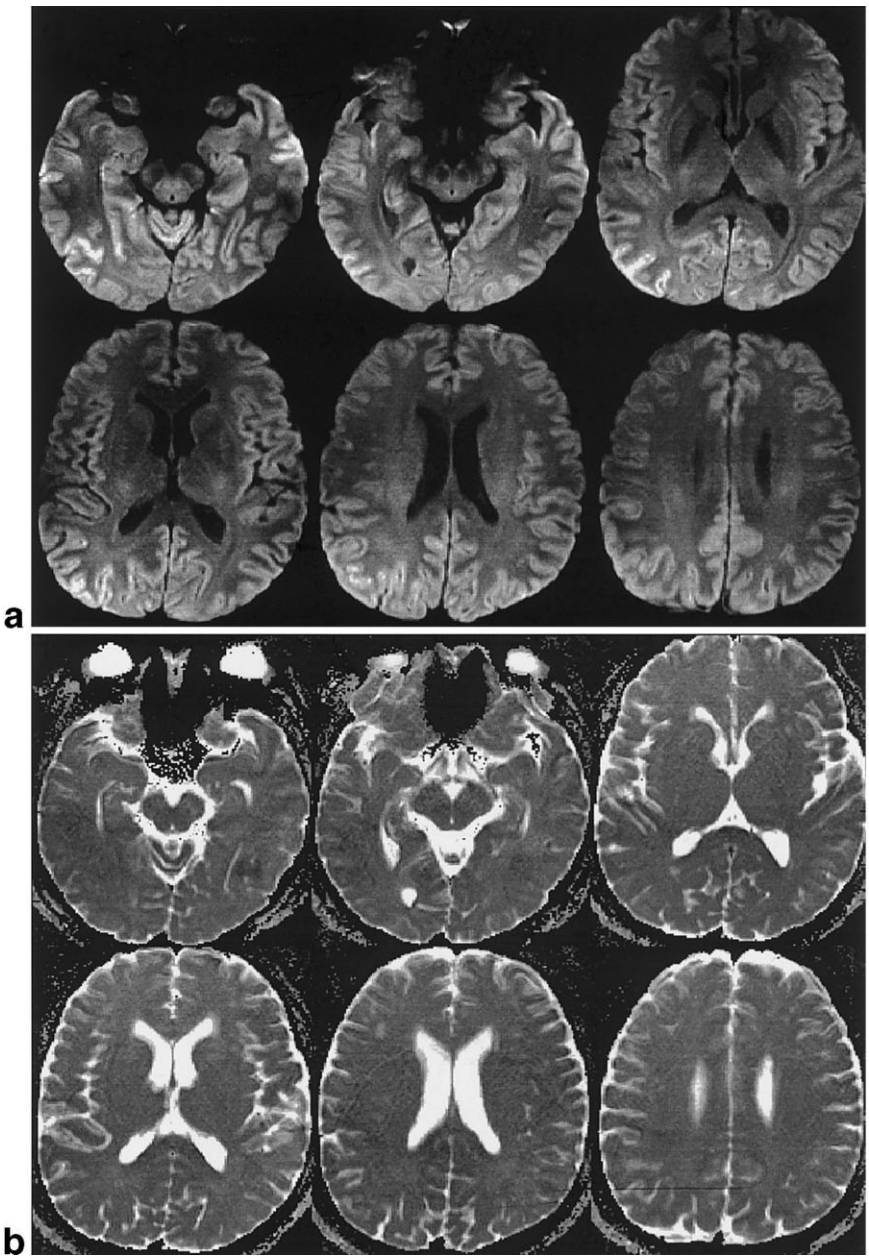


**Figure 6.** The isotropic diffusion-weighted images (**a**) at b = 1000 seconds/mm$^2$ acquired using 32 interleaves of variable-density spiral method and the corresponding ADC maps (**b**). The following acquisition parameters were used: $B_0$ = 3 T, TE/TR = 80/6000 msec, FOV = 230 mm, matrix size = 256 × 256, and slice thickness = 3 mm. Both the diffusion-weighted images (a) and ADC maps (b) are the average results from the measurements using the tetrahedral gradient set and are equivalent to the average results from an infinite number of diffusion-weighting directions.

brain with DTI. For example, very small lesions of 1–2 mm in size could be missed or blurred out in low-resolution images based on single-shot techniques (7,12). The limited spatial resolution and SNR also pose a severe problem for clinical applications of DTI, because minor structural changes in the white matter associated with neuropsychiatric disorders cannot be reliably detected with single-shot techniques (5). For future development, we will combine this multishot variable-density spiral sequence for DWI with some optimized DTI schemes (26) for high-resolution DTI studies.

In conclusion, the preliminary results from this study demonstrate that self-navigated multishot DWI based on the variable-density spiral trajectory design is adequately robust to acquire high-resolution diffusion-weighted images without the need of excessive head restraint and cardiac gating. This acquisition method oversamples the central k-space densely in each interleave and allows for self-navigated motion correction. Further enhancement of the robustness against motion artifacts can be achieved by exclusion of corrupted data acquisition due to out-of-plane or excessive in-plane motions. When the motion artifact problem in DWI is solved, the multishot DWI technique has significant advantages, such as good spatial resolution and reduced magnetic susceptibility artifacts. The implementation of this time-efficient k-space sampling method is highly simplified by using the closed-form approximation for on-line waveform calculation. The solution remains well behaved in the both gradient slew-rate- and amplitude-limited regions. The ability to calculate readout waveforms using an analytical formula provides flexibility to test scanning protocols and hardware characteristics.

Table 2
The Average ADC ± SD in $10^{-3}$ $mm^2$/seconds for the Phantom and Individual Subjects*

| | $N = 8$ | $N = 16$ | $N = 32$ |
|---|---|---|---|
| Gel phantom | 1.67 ± 0.09 | 1.65 ± 0.09 | 1.66 ± 0.08 |
| Subject 1[a] | 0.90 ± 0.07 | 0.91 ± 0.08 | 0.91 ± 0.06 |
| Subject 2[a] | 0.93 ± 0.07 | 0.93 ± 0.08 | 0.92 ± 0.07 |
| Subject 3[a] | 0.92 ± 0.09 | 0.91 ± 0.07 | 0.90 ± 0.06 |
| Intersubject | 0.92 ± 0.02 | 0.92 ± 0.02 | 0.91 ± 0.01 |

*The SDs were based on three repeated measurements of the average ADC which in term was the average result from the measurements of tetrahedral gradient set.
[a]The in vivo ADC results were evaluated from at least six brain ROIs carefully selected to void cerebral spinal fluid.

## REFERENCES


1. Moseley ME, Butts K, Yenari MA, Marks M, de Crespigny A. Clinical aspects of DWI. NMR Biomed 1995;8:387–396.
2. Conturo TE, Lori NF, Cull TS, et al. Tracking neuronal fiber pathways in the living human brain. Proc Natl Acad Sci USA 1999;96: 10422–10427.
3. Mori S, Crain BJ, Chacko VP, van Zijl PC. Three-dimensional tracking of axonal projections in the brain by magnetic resonance imaging. Ann Neurol 1999;45:265–269.
4. Basser PJ, Pajevic S, Pierpaoli C, Duda J, Aldroubi A. In vivo fiber tractography using DT-MRI data. Magn Reson Med 2000;44:625–632.
5. Li TQ, Noseworthy MD. Mapping the development of white matter tracts with diffusion tensor imaging. Dev Sci 2002;5:293–300.
6. Klingberg T, Hedehus M, Temple E, et al. Microstructure of temporo-parietal white matter as a basis for reading ability: evidence from diffusion tensor magnetic resonance imaging. Neuron 2000; 25:493–500.
7. Butts K, Pauly J, de Crespigny A, Moseley M. Isotropic diffusion-weighted and spiral-navigated interleaved EPI for routine imaging of acute stroke. Magn Reson Med 1997;38:741–749.
8. Glover GH. Simple analytic spiral K-space algorithm. Magn Reson Med 1999;42:412–415.
9. Nishimura DG, Irarrazabal P, Meyer CH. A velocity k-space analysis of flow effects in echo-planar and spiral imaging. Magn Reson Med 1995;33:549–556.
10. Li TQ, Takahashi AM, Hindmarsh T, Moseley ME. ADC mapping by means of a single-shot spiral MRI technique with application in acute cerebral ischemia. Magn Reson Med 1999;41:143–147.
11. Brockstedt S, Thomsen C, Wirestam R, Holtas S, Stahlberg F. Quantitative diffusion coefficient maps using fast spin-echo MRI. Magn Reson Imaging 1998;16:877–886.
12. Pipe JG, Farthing VG, Forbes KP. Multishot diffusion-weighted FSE using PROPELLER MRI. Magn Reson Med 2002;47:42–52.
13. Ordidge RJ, Helpern JA, Qing ZX, Knight RA, Nagesh V. Correction of motional artifacts in diffusion-weighted MR images using navigator echoes. Magn Reson Imaging 1994;12:455–460.
14. de Crespigny AJ, Marks MP, Enzmann DR, Moseley ME. Navigated diffusion imaging of normal and ischemic human brain. Magn Reson Med 1995;33:720–728.
15. Anderson AW, Gore JC. Analysis and correction of motion artifacts in diffusion weighted imaging. Magn Reson Med 1994;32:379–387.
16. Meyer CH, Hu BS, Nishimura DG, Macovski A. Fast spiral coronary artery imaging. Magn Reson Med 1992;28:202–213.
17. Tsai CM, Nishimura DG. Reduced aliasing artifacts using variable-density k-space sampling trajectories. Magn Reson Med 2000;43: 452–458.
18. Nayak KS, Tsai CM, Meyer CH, Nishimura DG. Efficient off-resonance correction for spiral imaging. Magn Reson Med 2001;45: 521–524.
19. Miller KL, Pauly JM. Nonlinear phase correction for navigated diffusion imaging. Magn Reson Med 2003;50:343–353.
20. Kim DH, Adalsteinsson E, Spielman DM. Simple analytic variable density spiral design. Magn Reson Med 2003;50:214–219.
21. Adalsteinsson E, Star-Lack J, Meyer CH, Spielman DM. Reduced spatial side lobes in chemical-shift imaging. Magn Reson Med 1999;42:314–323.
22. Conturo TE, McKinstry RC, Akbudak E, Robinson BH. Encoding of anisotropic diffusion with tetrahedral gradients: a general mathematical diffusion formalism and experimental results. Magn Reson Med 1996;35:399–412.
23. Pipe JG. Motion correction with PROPELLER MRI: application to head motion and free-breathing cardiac imaging. Magn Reson Med 1999;42:963–969.
24. Miller KL, Meyer CH, Pauly JM. Self-navigated spirals for high resolution steady-state diffusion imaging. In: Proceedings of the 10th Annual Meeting of ISMRM, Honolulu, 2002.10:1110.
25. Conturo TE, McKinstry RC, Aronovitz JA, Neil JJ. Diffusion MRI: precision, accuracy and flow effects. NMR Biomed 1995;8:307–332.
26. Skare S, Hedehus M, Moseley ME, Li TQ. Condition number as a measure of noise performance of diffusion tensor data acquisition schemes with MRI. J Magn Reson 2000;147:340–352.